

# Surface-state Coulomb repulsion accelerates a metal-insulator transition in topological semimetal nanofilms

S. Ito,<sup>1</sup> M. Arita,<sup>2</sup> J. Haruyama,<sup>1</sup> B. Feng,<sup>3</sup> W.-C. Chen,<sup>4</sup> H. Namatame,<sup>2</sup> M. Taniguchi,<sup>2</sup> C.-M. Cheng,<sup>4</sup> G. Bian,<sup>5</sup> S.-J. Tang,<sup>4,6</sup> T.-C. Chiang,<sup>7</sup> O. Sugino,<sup>1</sup> F. Komori,<sup>1</sup> and I. Matsuda<sup>1</sup>

<sup>1</sup>*Institute for Solid State Physics (ISSP), The University of Tokyo, Kashiwa, Chiba 277-8581, Japan*

<sup>2</sup>*Hiroshima Synchrotron Radiation Center (HSRC), Hiroshima University,  
2-313 Kagamiyama, Higashi-Hiroshima 739-0046, Japan*

<sup>3</sup>*Institute of Physics, Chinese Academy of Sciences, Beijing 100190, China*

<sup>4</sup>*National Synchrotron Radiation Center (NSRRC), Hsinchu, Taiwan 30076, Republic of China*

<sup>5</sup>*Department of Physics and Astronomy, University of Missouri, Columbia, Missouri 65211, USA*

<sup>6</sup>*Department of Physics and Astronomy, National Tsing Hua University, Hsinchu, Taiwan 30013, Republic of China*

<sup>7</sup>*Department of Physics and Frederick Seitz Materials Research Laboratory,  
University of Illinois at Urbana-Champaign, Urbana, Illinois 61801, USA*

(Dated: December 15, 2024)

The emergence of quantization at the nanoscale, the quantum size effect (QSE), allows flexible control of matter and is a rich source of advanced functionalities. A QSE-induced transition into an insulating phase in semimetallic nanofilms was predicted for bismuth a half-century ago and has regained new interest with regard to its surface states exhibiting nontrivial electronic topology. Here, we reveal an unexpected mechanism of the transition by high-resolution angle-resolved photoelectron spectroscopy combined with theoretical calculations. Anomalous evolution and degeneracy of quantized energy levels indicate that increased Coulomb repulsion from the surface states deforms a quantum confinement potential with decreasing thickness. The potential deformation drastically modulates spatial distributions of quantized wave functions, which leads to acceleration of the transition even beyond the original QSE picture. This discovery establishes a complete picture of the long-discussed problem in bismuth and highlights the new class of size effects dominating nanoscale transport in systems with metallic surface states.

Quantized electronic states generated by the quantum size effect (QSE) in nano-confined systems enable unique tunability for a wide range of phenomena such as superconductivity<sup>1</sup>, light-matter interaction<sup>2</sup>, and non-equilibrium carrier dynamics<sup>3</sup>. Modulations of the band gap and the density of states further improve functionalities in catalysts<sup>4</sup> and information devices<sup>5</sup>. From a technological point of view, quantization inevitably affects any electronic system fabricated at the nanoscale. One of the most well-known examples is a QSE-induced metal-insulator transition, whose essence is illustrated for a film geometry in Figs. 1a,b. When semimetallic bulk bands are quantized, the valence-band top and the conduction-band bottom no longer cross the Fermi level ( $E_F$ ), and the system enters an insulating phase. In the case of a system possessing metallic surface states as typically observed in topological materials, the transition is marked by the disappearance of conducting channels in the film interior, and thereafter an electric current flows only through the surfaces.

The transition was first predicted a half-century ago on bismuth (Bi)<sup>6</sup>. A Bi single crystal is a typical semimetal with small carrier pockets and three-dimensional (3D) Dirac dispersions<sup>7</sup>, which generate unusual magneto-transport responses<sup>8–10</sup>. Moreover, due to the large spin-orbit coupling, Bi surfaces host spin-polarized metallic states

(Figs. 1a,b,e) that have been intensively examined in the context of nontrivial electronic topology<sup>11–14</sup>. In particular, the surface states in a film are very recently identified as a nematic quantum Hall liquid<sup>15,16</sup>. The QSE-driven metal-insulator transition in Bi nanofilms, historically called a semimetal-semiconductor transition, originally received great attention as a nanoscale pathway for achieving a substantial thermoelectric figure of merit<sup>17</sup> and is now of interest for enhancing the surface-state-induced phenomena. Evidence of the transition was obtained only in this decade by transport measurements on epitaxially grown Bi thin films<sup>18–20</sup>. However, a recent angle-resolved photoelectron spectroscopy (ARPES) observation of electronic band structures detected a bulk-like envelope crossing  $E_F$  in atomically thin Bi films<sup>21</sup>, in clear contrast to transport results showing only an interior-insulating phase below a threshold thickness<sup>18–20</sup>. Although this strange contradiction between metallic and insulating behaviors observed in completely the same system implies the presence of an intriguing mechanism, essential quantization information was lacking in previous experiments.

Here, we report the first direct observation of the transition with all the quantized energy levels resolved by high-resolution ARPES of high-quality Bi films. Visualization of anomalous level evolution contrasted with tight-binding simulations highlights an additional mechanism beyond simple QSE. The high-resolution ARPES also detects unexpected degeneracy of top two quantized energy levels, which completely breaks a standard quantization rule. Furthermore, our systematic density-functional-theory (DFT) calculations reveal that the level degeneracy is gradually induced by shifting the whole band structure and accompanies transformation of the bulk-like wave functions into surface-localized ones. This tendency is totally opposite to a well-known hybridization effect between top and bottom surface states and perfectly reconciles the contradiction among previous experiments. These unusual modulations of quantized bulk states can be fully explained only when we consider deformation of a quantum confinement potential, which is triggered by enhanced effects of Coulomb repulsion with decreasing system size, centering on a size-independent contribution from the surface states. The present study not only solves the serious controversy on the transition discussed for half a century but also introduces the novel size effect which can be universally present in a system with metallic surface states, typically topological materials.

Figures 1f,g show Fermi surfaces and band structures measured for a 14 bilayer (BL) Bi film (1 BL = 3.93 Å). Two

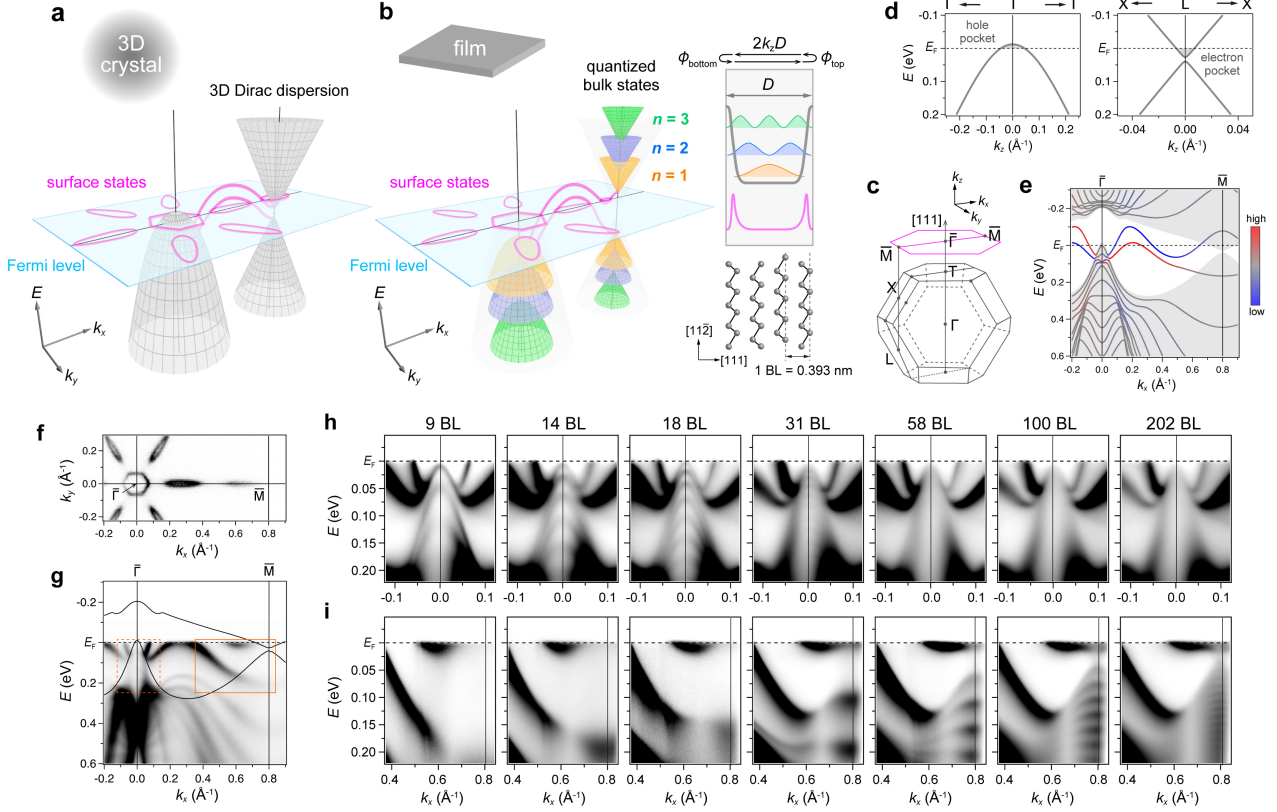


FIG. 1. **First direct observation of a QSE-induced metal-insulator transition.** **a,b,** Schematic of the metal-insulator transition in a Bi nanofilm. While 3D bulk states become quantized and gapped across the Fermi level, metallic surface states remain intact. The inset of **(b)** depicts wave function characters of the surface states and the quantized bulk states formed inside a film with thickness  $D$ . Circulating arrows show a boundary condition for the latter, where  $\phi_{\text{top}}$  and  $\phi_{\text{bottom}}$  are phase shifts when reflected at top and bottom surfaces. The drawing below also illustrates a bilayer (BL) structure of Bi. **c,** Bulk and surface Brillouin zone of Bi in the  $[111]$  direction. **d,** Bi bulk band structures calculated around the hole and electron pockets using a tight-binding method. **e,** Band structures obtained by a tight-binding calculation for a 14 BL Bi(111) slab. The color scale shows in-plane spin-polarization of two surface-state bands in the direction perpendicular to  $\bar{\Gamma}\bar{M}$ . **f,g,** Experimental Fermi surfaces and band structures measured along  $\bar{\Gamma}\bar{M}$  on a 14 BL Bi(111) film grown on a Ge(111) substrate. Shaded areas in **(e)** and solid curves in **(g)** show calculated bulk projections. **h,i** Experimental band structures magnified inside dashed and solid boxes in **(g)**, respectively, for each thickness.

spin-polarized surface-state bands and quantized bulk bands are distinctly observed in excellent agreement with those calculated in Fig. 1e. In Figs. 1h,i, we systematically follow the evolution of the band structures around the hole and electron pockets with increasing thickness. The valence-band top at  $\bar{\Gamma}$  is resolved with all the quantized bands and is located well below  $E_F$  in atomically thin films. Interestingly, this is in contrast to the previous ARPES result<sup>21</sup> and is attributed to a lattice strain effect as discussed later. The conduction-band bottom at  $\bar{M}$  shifts upwards with decreasing thickness (see also Supplementary Section B) and it is now clear that the bulk band edges no longer cross  $E_F$  and that we observe the first direct ARPES evidence of the metal-insulator transition.

Furthermore, we follow the evolution of the quantized energy levels to investigate mechanisms of the transition, as shown with energy distribution curves (EDCs) at  $\bar{M}$  and  $\bar{\Gamma}$  in Figs. 2a,b. The energy position of each level is described by a boundary condition of confined wave functions<sup>22</sup>:

$$2k_z D + \Phi = 2\pi(n - 1) \quad (1)$$

where  $k_z$  is a wavenumber in the surface-normal direction;  $D$  is a film thickness;  $\Phi$  is the total phase shift  $\phi_{\text{top}} + \phi_{\text{bottom}}$ , as illustrated in Fig. 1b. Eq. (1) tells us that the wavenumber is proportional to the inverse thickness:

$$k_z = \left\{ \pi(n - 1) - \frac{\Phi}{2} \right\} \frac{1}{D}. \quad (2)$$

Therefore, a plot of quantized energy levels vs. inverse thicknesses depicts a bulk band dispersion perpendicular to the film surface. At  $\bar{M}$ , the corresponding direction has the Dirac dispersion of Bi (Fig. 1c,d). Figure 2c shows that evolutions of the peaks are perfectly reproduced by linear functions based on Eq. (2) and a constant phase shift value  $\Phi$  obtained in ref.<sup>13</sup>. However, at  $\bar{\Gamma}$ , with a parabolic surface-normal dispersion, the peak evolutions are far from the predictions and can be fitted only by a parabolic function with an additional exponential term as shown in Fig. 2d (see Supplementary Section C for the details of the fitting). This situation becomes more evident when compared to tight-binding calculations with a slab geometry<sup>23</sup> in Fig. 2e, where only pure QSE is implemented.

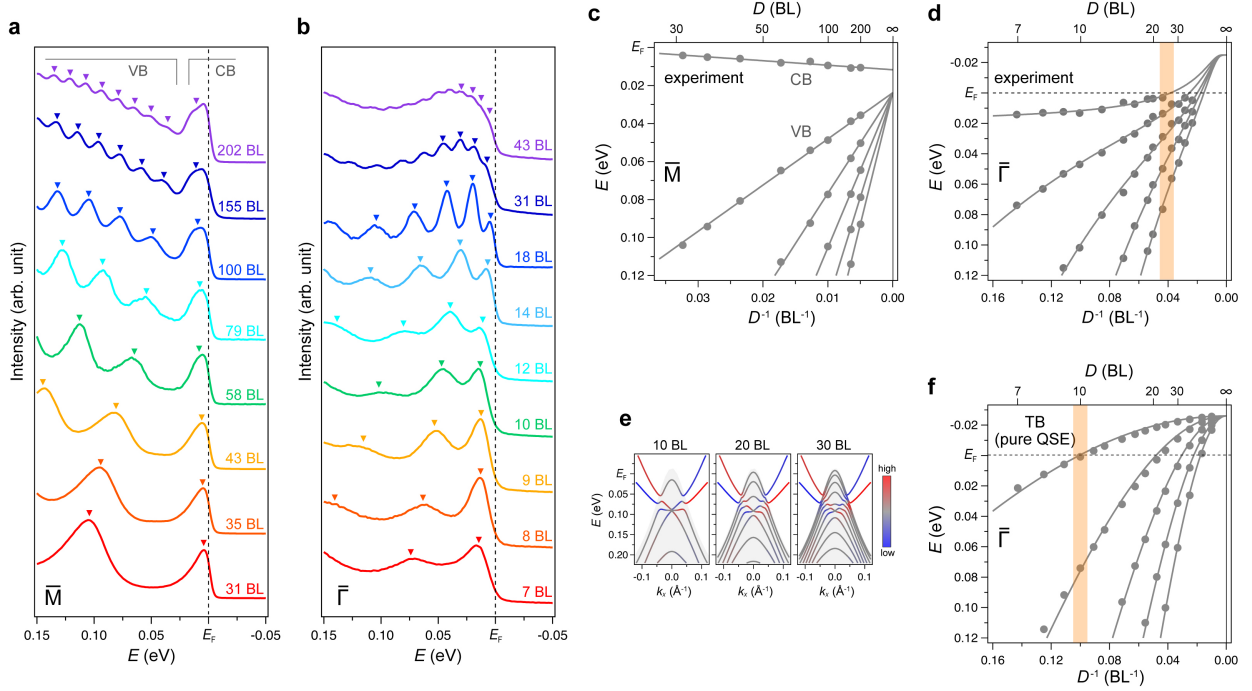


FIG. 2. **Anomalous evolution of quantized energy levels observed in the atomically thin regime.** **a,b,** Evolution of energy distribution curves (EDCs) extracted at  $\bar{M}$  and  $\bar{\Gamma}$  for each thickness. Markers show peak positions determined by Lorentzian fitting. Peaks belonging to the conduction band (CB) and the valence band (VB) are also denoted in **(a)**. **c,** Peak positions at  $\bar{M}$  vs. inverse thicknesses of each film. Linear functions are based on Eq. (2) with a surface-normal band dispersion and a phase shift obtained experimentally<sup>13</sup>. **d,** The same as **(c)** for peak positions at  $\bar{\Gamma}$ . Solid curves are fitting functions discussed in the main text and Supplementary Section C. A shaded bar highlights a thickness where the top quantized level crosses  $E_F$ . **e,** Evolution of band structures around  $\bar{\Gamma}$  calculated by a tight-binding method for Bi slabs. The color scale is the same as in Fig. 1(d). **f,** The same as **(d)** for energy levels obtained by the tight-binding calculations that reflect only pure QSE.

In this case, all the peak evolutions in Fig. 2f are consistently described by parabolic functions, which again supports the validity of Eq. (2) with constant  $\Phi$ . The striking contrast between these two cases indicates that an additional size effect beyond a primitive QSE is driving this anomalous evolution in atomically thin regions. This leads to enhancement of the critical thickness where the top quantized level crosses  $E_F$ , as highlighted by shaded bars in Fig. 2d,f.

Another unusual signature appears in the precise resolution of the band structures. Figure 3a shows peak-enhanced ARPES images for atomically thin films, where both surface-state bands connect to the top quantized bulk band. Because there are states localized at the top and bottom surfaces, these surface-state bands are doubly degenerate in the nearly free-standing film (see Supplementary Section D). This band connection thus indicates that the top quantized level must be quadruply degenerate. That is,  $n = 1$  and 2 quantized levels are almost degenerate (Fig. 3b), which has never been reported in ARPES experiments of thin films.

Nevertheless, the observations can be reproduced by first-principles calculations that systematically shift the entire band structures, as shown in Fig. 3c. The shifts are manually induced by changing lattice parameters, where the in-plane lattice constant is modulated by -2, -1, 0, +1 % from left to right, respectively. Along with the shift toward a higher binding energy, the energy separation between  $n = 2$  and 3 levels increases. In contrast, the separation between  $n = 1$  and 2 levels is reduced; their eventual degeneracy is consistent with Fig. 3a,b. It is as if the quantized bands split off from the bulk

projection and behave independently as surface-state bands. This is supported by examining wave functions for each quantized state in Fig. 3d. In the left panel, the wave functions have envelope shapes expected for  $n = 1, 2, 3$  states confined in a quantum well. However, as the unusual level degeneracy appears, wave functions of  $n = 1$  and 2 states are transformed into surface-localized ones. It is well known that electronic states localized on top and bottom surfaces can hybridize and exhibit a bulk-like character in atomically thin films<sup>24,25</sup>; however, the complete opposite, transformation of bulk-like states into surface-localized ones, is observed here.

An important question is what is the central mechanism responsible for the anomalous behaviors. The level degeneracy rules out major contributions of standard size effects related to charge transfer, lattice strain, and recently proposed surface-size effects<sup>21</sup>, all of which only uniformly shifts or expands the quantized bands. Note that the lattice strain effect corresponds to a uniform compression/expansion of in-plane/out-of-plane lattice constants due to a lattice mismatch with substrates. We can still think of modulation in the interlayer spacing, which can affect Bi band structures to a relatively large extent<sup>26</sup>. However, this effect is also excluded as the central mechanism of the present observations because our DFT calculations already exhibit the level degeneracy and the bulk-to-surface transformation without any modulation of the interlayer spacing implemented.

Although the transformation of  $n = 1$  and 2 confined wave functions into surface-like states can be viewed as a result of hybridization between the surface and bulk states around  $\bar{\Gamma}$ ,

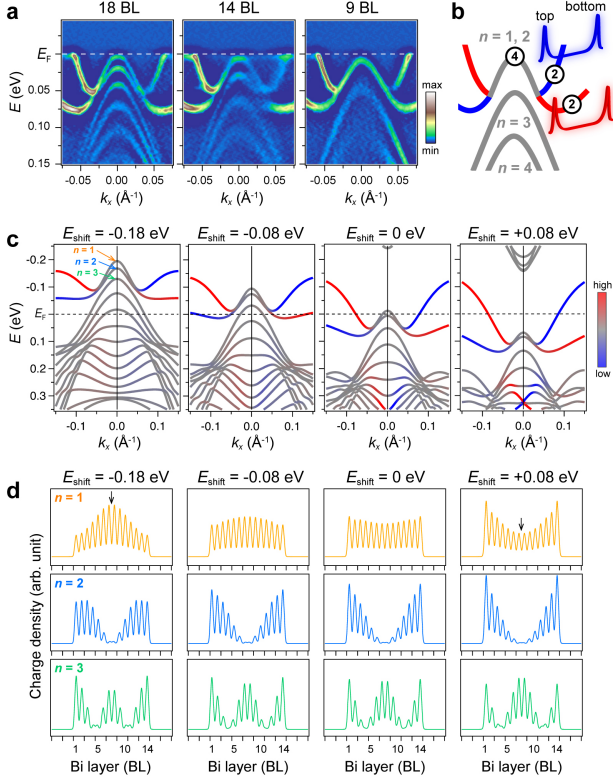


FIG. 3. **Unexpected level degeneracy and bulk-to-surface transformation.** **a**, Second derivative ARPES images for highlighting peak positions around  $\bar{\Gamma}$  in atomically thin Bi films. **b**, Schematic of unusual band connections between the top quantized band and the surface-state bands. The number of states in each band is explicitly shown with illustrations of wave functions localized near the top and bottom surfaces. **c**, Evolution of band structures shifted in energy by tuning lattice parameters in first-principles calculations of a 14 BL Bi slab. The color scale depicts spin-polarization in the same manner as in Fig. 1(d). **d**, Squared values of wave functions for  $n = 1, 2, 3$  states at  $\bar{\Gamma}$  in (c). The horizontal axis corresponds to the direction perpendicular to the slab surface, where in-plane contributions are integrated.

the reason for the degeneracy between these two quantized bulk states is not yet accounted for. More importantly, we need to address the reason why the level degeneracy and the bulk-to-surface transformation are gradually induced by shifting the whole band structure in Fig. 3c,d. Band shifts induced by lattice-parameter modulation cannot explain them as confirmed by tight-binding calculations (see Supplementary Section D). An essential difference between the present tight-binding and first-principles approaches is implementation of Coulomb interaction. In the general framework of DFT, an effective one-body potential  $V_{\text{eff}}$  and a total charge density  $n_{\text{total}}$  are determined by a self-consistent cycle reflecting Coulomb interaction via the Hartree functional and the exchange-correlation functional<sup>27</sup>. Here, the occupation of the surface-state bands increases from left to right in Fig. 3c, which increases their relative contributions to the total charge density  $n_{\text{total}} = n_{\text{surface}} + n_{\text{interior}}$ : this can modify the effective potential  $V_{\text{eff}}$  and electronic structures finally obtained.

We further conceive that Coulomb repulsion among electrons tends to compress the total charge distribution toward the film center when the surface contributions increase. The

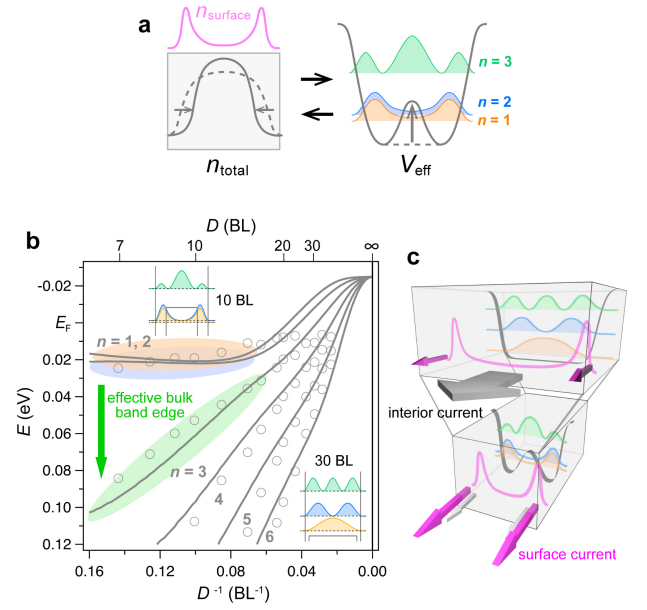


FIG. 4. **Surface-state Coulomb repulsion induces deformation of a quantum confinement potential.** **a**, Schematic of a self-consistent cycle for a total charge density  $n_{\text{total}}$  and an effective confinement potential  $V_{\text{eff}}$ , which is triggered by increased contributions of surface states and concomitant compression of the total charge distribution via Coulomb repulsion. Energy levels and wave function characters of eigenstates in a double-well potential are also illustrated. **b**, Solid curves: evolution of quantized energy levels simulated using an ideal quantum-well potential subject to a gradual double-well modulation. Markers show experimental data corrected for standard size effects (see Supplementary Section D). The insets show squared values of wave functions that are calculated for 10 BL and 30 BL cases. **c**, Schematic representation of the novel size effect dominating nanoscale electronic transport in a system with metallic surface states, centering on a size-independent contribution from the surface states.

behavior is indeed observed in the present calculations (see Supplementary Section E). In the one-body picture of the DFT framework, the compressed total charge in turn makes an electron feel a potential barrier around the film center and deforms  $V_{\text{eff}}$  into a double-well-like shape, as illustrated in Fig. 4a. Eigenstates of a double-well potential have nearly degenerate ground states with wave functions localized in each well; this then provides a qualitative explanation of the experimental observations. In real Bi films, the positions of the surface-state bands are almost independent of thicknesses (Fig. 1h,i). Nevertheless, reducing the system size increases relative contributions of the surface states to the total charge density, which has essentially the same effect. We also examine this picture by performing a numerical simulation using a 1D Schrödinger equation with an ideal quantum-well potential that is gradually deformed to a double well. Figure 4b shows that this simple model quantitatively reproduces both the anomalous evolution and the level degeneracy when a double-well modulation and the resulting change in a band dispersion (an effective mass) have an exponential thickness dependence (see Supplementary Section F). The insets also demonstrate that the wave functions are indeed transformed to surface-localized ones with decreasing thickness.

Thus, the two essential signatures here, the degeneracy between top two quantized bulk states and their transformation into surface-localized states, rule out scenarios given by any standard mechanism but are naturally explained by considering the deformation of a quantum confinement potential via Coulomb repulsion from the surface states. One of the most interesting points is that a usually weak effect of Coulomb repulsion and hybridization between the surface and quantized bulk states are enhanced with decreasing system size centering on the presence of the surface states.

Finally, we revisit the strange contradiction among recent studies on the metal-insulator transition in Bi films. The central problem is a metallic envelope of quantized bulk states captured by the previous ARPES of atomically thin Bi films grown on a Si(111) substrate<sup>21</sup>, whose film interiors were insulating in the transport experiments<sup>18–20</sup>. Using the same substrate, we reproduced this ARPES data. The smaller Si lattice constant relative to that of Ge exerts compressive strain and shifts the whole band structure upwards so that the top quantized level crosses  $E_F$  (see Supplementary Section D). However, as shown in Fig. 3d and in the insets of Fig. 4b, the wave function of this top quantized level behaves like a surface-conducting channel, and the resulting shift of an effective band edge makes the system interior-insulating even in the Bi/Si case, which is consistent with the transport experiments<sup>18–20</sup>. Therefore, in addition to the exponential level evolution pushed by the emergent double-well potential (Fig. 2d,f), the bulk-to-surface transformation further accelerates the metal-insulator transition. This is the complete picture of the long-discussed problem in Bi, whose mechanism is unexpectedly extended beyond the standard QSE scenario.

The present conclusion can be generalized to a new class of size effects in any dimension, where increased contributions of one- and two-dimensional edge states with decreasing system size modify an effective one-body potential via Coulomb repulsion. Here, the first experimental signature on a specific system still calls for more detailed theoretical studies in a wide range of materials. Nevertheless, the comprehensive discussions presented above suggest that the effect is likely to be present in a universal system with metallic edge states. A target of the greatest interest will be nanofilms of recently discovered Dirac<sup>28</sup>, Weyl<sup>29,30</sup>, and topological nodal-line semimetals<sup>31</sup> that inherently possess metallic edge states and a small number of bulk carriers near  $E_F$  inside their point-/loop-like semimetallic nodes. Nano-fabrication of such topological semimetals is an indispensable step for their device applications, in which various size effects including the one discovered here will play an essential role and provide new control parameters for advanced functionalities.

**Acknowledgements** We thank Prof. T. Hirahara and Prof. M. Horn-von Hoegen for valuable discussions on the growth of Bi films. We also thank Prof. T. Kato, Dr. Y. Konishi, and Dr. T. Miyamachi for fruitful discussions on edge states in a confined geometry. We acknowledge Prof. T. Aono, Dr. Y. Ohtsubo and Dr. R. Yukawa for advice on theoretical calculations. We thank Dr. Alan Burns from the Edanz Group for checking a draft of the manuscript. The ARPES measurements were performed with the approval of the Proposal Assessing Committee of HSRC (Project No. 15-A-38, 17AU025, and 18AU008) and the Proposal Assessing Com-

mittee of NSRRC (Project No. 2015-2-090-1). I.M. acknowledges support by JSPS under KAKENHI Grant No. 18H03874. T.C.C. acknowledges support from the U.S. National Science Foundation under grant number DMR-17-09945. S.I. acknowledges support by JSPS under KAKENHI Grant No. 17J03534. S.I. was also supported by JSPS through the Program for Leading Graduate Schools (ALPS).

**Author Contributions** S.I. and I.M. planned the experimental project. S.I. fabricated thin film samples, conducted ARPES experiments, and analyzed the data. M.A., B.F., W.C.C., C.M.C. supported the ARPES experiments. S.I. performed tight-binding and model calculations. S.I. also performed first-principles calculations with support by G.B., J.H., and O.S. S.I. and I.M. wrote the paper. All authors contributed to discussions on the results and commented on the manuscript.

**Competing Interests** The authors declare no competing financial interests.

**Correspondence** Correspondence and requests for materials should be addressed to S.I. (email: s-ito@issp.u-tokyo.ac.jp) and I.M. (email: imatsuda@issp.u-tokyo.ac.jp).

## Methods

**Sample preparation.** Bi(111) films were grown epitaxially on a medium-doped p-type Ge(111) wafer cleaned by cycles of Ar<sup>+</sup> sputtering and annealing at 900 K. Bi evaporation was performed at room temperature, followed by annealing at 400 K<sup>32,33</sup>. To improve the film quality, the Ge substrate was prepared with large domains by fully outgassing the preparation systems and uniformly sputtering and annealing the substrate. The temperature during the Bi deposition was also carefully controlled. The relative accuracy of film thicknesses was precisely controlled using a quartz thickness monitor, and absolute film thicknesses were calibrated by comparing quantized energy levels with previous reports<sup>34–36</sup>.

**ARPES measurements.** High-resolution ARPES measurements were performed at BL-9A of the Hiroshima Synchrotron Radiation Center (HSRC) and BL-21B1 of the National Synchrotron Radiation Research Center (NSRRC). At BL-9A, a high-intensity unpolarized Xe plasma discharge lamp (8.437 eV) was used for magnifying small energy ranges, in addition to the synchrotron radiation (21 eV) for wide-range observations. The measurement temperature was 10 K, and the total energy resolution was 7 meV for 8.437 eV photons and 12 meV for 21 eV photons. The pressure during the measurements was  $2 \times 10^{-9}$  Pa. The measurement direction was precisely adjusted using an automated 6-axis rotational controller, and was based on Fermi surfaces that were mapped before every band-structure scan (see Supplementary Section A). To directly determine unoccupied band structures, we also performed alkali-metal adsorption following an approach in ref.<sup>37</sup> (see Supplementary Section B). We note that error bars are basically omitted in experimental plots because the scales are smaller than markers.

**Tight-binding calculations.** Tight-binding calculations for bulk electronic structures of Bi were based on a framework introduced in ref.<sup>38</sup>, which considers a  $16 \times 16$  matrix composed of hopping parameters of the  $sp^3$  orbitals between first-



, second-, and third-nearest neighbor atoms with spin-orbit coupling implemented. Electronic structures in a slab geometry were calculated by extending the bulk matrix to a larger  $16N \times 16N$  matrix, where  $N$  is the number of bilayers, as demonstrated in ref.<sup>23,39</sup>. The lattice parameters describing a Bi rhombohedral unit cell and the hopping parameters were taken from ref.<sup>38</sup>. The surface potential term was also introduced using formulations and parameters in ref.<sup>23</sup>.

**First-principles calculations.** Density functional theory (DFT) calculations<sup>27</sup> were performed with the ABINIT code<sup>40</sup>. The Perdew-Burke-Ernzerhof generalized gradient approximation was selected for the exchange-correlation functional<sup>41</sup>. A Hartwigsen-Goedecker-Hutter norm-conserving pseudopotential was used, in which spin-orbit coupling was implemented<sup>42</sup>. A free-standing Bi slab with a 14 BL thickness was used, and the length of a vacuum region was set to 8 BL (31.5 Å). Lattice parameters of the slab were fixed to the experimental values<sup>38</sup>. A Monkhorst-Pack grid for  $k$ -point sampling as  $9 \times 9 \times 1$  was used<sup>43</sup>. Convergences

with respect to an energy-cutoff, the  $k$ -point sampling, and the vacuum length were confirmed for obtained band structures. We also cross-checked the results using the QUANTUM-ESPRESSO code<sup>44</sup> with similar conditions.

**Model calculations.** A numerical simulation was performed using a 1D Schrödinger equation with an electron mass extracted from the tight-binding band structure. Eigenvalues were calculated by taking the Fourier transform of a wave function  $\phi(z) = \sum_{i=1}^{\infty} \sqrt{\frac{2}{L}} \alpha_i \sin(\frac{i\pi}{L}z)$  where  $L$  is a maximum length scale of the simulation<sup>45</sup>. A finite-height single-well potential was set inside this length scale. A double-well deformation of the single well was introduced with an exponential dependence on thickness. To manually simulate modulation of a band dispersion accompanying the potential deformation, an exponential dependence was also installed for the electron effective mass. All the parameters were adjusted to best fit the experimental data. Further details are described in Supplementary Section F.

- <sup>1</sup> Guo, Y. *et al.* Superconductivity modulated by quantum size effects. *Science* **306**, 1915–1917 (2004).
- <sup>2</sup> Campos, A. *et al.* Plasmonic quantum size effects in silver nanoparticles are dominated by interfaces and local environments. *Nature Physics* **15**, 275–280 (2018).
- <sup>3</sup> Kirchmann, P. S. *et al.* Quasiparticle lifetimes in metallic quantum-well nanostructures. *Nature Physics* **6**, 782–785 (2010).
- <sup>4</sup> Lopez-Acevedo, O., Kacprzak, K. A., Akola, J. & Häkkinen, H. Quantum size effects in ambient CO oxidation catalysed by ligand-protected gold clusters. *Nature Chemistry* **2**, 329–334 (2010).
- <sup>5</sup> Mahendra, D. *et al.* Room-temperature high spin-orbit torque due to quantum confinement in sputtered  $\text{Bi}_x\text{Se}_{1-x}$  films. *Nature Materials* **17**, 800–807 (2018).
- <sup>6</sup> Sandomirskii, V. B. Quantum size effect in a semimetal film. *Sov. Phys. JETP* **25**, 101–106 (1967).
- <sup>7</sup> Hofmann, P. The surfaces of bismuth: Structural and electronic properties. *Prog. Surf. Sci.* **81**, 191–245 (2006).
- <sup>8</sup> Li, L. *et al.* Phase transitions of dirac electrons in bismuth. *Science* **321**, 547–550 (2008).
- <sup>9</sup> Zhu, Z., Collaudin, A., Fauqué, B., Kang, W. & Behnia, K. Field-induced polarization of dirac valleys in bismuth. *Nature Physics* **8**, 89–94 (2012).
- <sup>10</sup> Küchler, R. *et al.* Thermodynamic evidence for valley-dependent density of states in bulk bismuth. *Nature Materials* **13**, 461–465 (2014).
- <sup>11</sup> Ohtsubo, Y. *et al.* Non-trivial surface-band dispersion on Bi(111). *New J. Phys.* **15**, 033041 (2013).
- <sup>12</sup> Drozdov, I. K. *et al.* One-dimensional topological edge states of bismuth bilayers. *Nature Physics* **10**, 664–669 (2014).
- <sup>13</sup> Ito, S. *et al.* Proving nontrivial topology of pure bismuth by quantum confinement. *Phys. Rev. Lett.* **117**, 236402 (2016).
- <sup>14</sup> Schindler, F. *et al.* Higher-order topology in bismuth. *Nature Physics* **14**, 918–925 (2018).
- <sup>15</sup> Feldman, B. E. *et al.* Observation of a nematic quantum hall liquid on the surface of bismuth. *Science* **354**, 316–321 (2016).
- <sup>16</sup> Randeria, M. T. *et al.* Interacting multi-channel topological boundary modes in a quantum hall valley system. *Nature* **566**, 363–367 (2019).
- <sup>17</sup> Dresselhaus, M. S. *et al.* New directions for low-dimensional thermoelectric materials. *Advanced Materials* **19**, 1043–1053 (2007).
- <sup>18</sup> Xiao, S., Wei, D. & Jin, X. Bi(111) thin film with insulating interior but metallic surfaces. *Phys. Rev. Lett.* **109**, 166805 (2012).
- <sup>19</sup> Zhu, K., Wu, L., Gong, X., Xiao, S. & Jin, X. Quantum transport in the surface states of epitaxial Bi(111) thin films. *Phys. Rev. B* **94**, 121401 (2016).
- <sup>20</sup> Kröger, P. *et al.* Controlling conductivity by quantum well states in ultrathin Bi(111) films. *Phys. Rev. B* **97**, 045403 (2018).
- <sup>21</sup> Hirahara, T. *et al.* Role of quantum and surface-state effects in the bulk fermi-level position of ultrathin Bi films. *Phys. Rev. Lett.* **115**, 106803 (2015).
- <sup>22</sup> Chiang, C., T. Photoemission studies of quantum well states in thin films. *Surf. Sci. Rep.* **39**, 181–235 (2000).
- <sup>23</sup> Saito, K., Sawahata, H., Komine, T. & Aono, T. Tight-binding theory of surface spin states on bismuth thin films. *Phys. Rev. B* **93**, 041301 (2016).
- <sup>24</sup> Hirahara, T. *et al.* Origin of the surface-state band-splitting in ultrathin Bi films: from a Rashba effect to a parity effect. *New J. Phys.* **10**, 083038 (2008).
- <sup>25</sup> Zhang, Y. *et al.* Crossover of the three-dimensional topological insulator  $\text{Bi}_2\text{Se}_3$  to the two-dimensional limit. *Nature Physics* **6**, 584–588 (2010).
- <sup>26</sup> Koroteev, Y. M., Bihlmayer, G., Chulkov, E. V. & Blügel, S. First-principles investigation of structural and electronic properties of ultrathin Bi films. *Phys. Rev. B* **77**, 045428 (2008).
- <sup>27</sup> Martin, R. M. *Electronic structure: basic theory and practical methods* (Cambridge university press, Cambridge, 2004).
- <sup>28</sup> Liu, Z. K. *et al.* Discovery of a three-dimensional topological Dirac semimetal,  $\text{Na}_3\text{Bi}$ . *Science* **343**, 864–867 (2014).
- <sup>29</sup> Xu, S.-Y. *et al.* Discovery of a Weyl fermion semimetal and topological Fermi arcs. *Science* **349**, 613–617 (2015).
- <sup>30</sup> Lv, B. Q. *et al.* Experimental discovery of Weyl semimetal TaAs. *Phys. Rev. X* **5**, 031013 (2015).
- <sup>31</sup> Bian, G. *et al.* Topological nodal-line fermions in spin-orbit metal  $\text{PbTaSe}_2$ . *Nature Commun.* **7**, 10556 (2016).
- <sup>32</sup> Hatt, S., Ohtsubo, Y., Miyamoto, S., Okuyama, H. &

- Aruga, T. Epitaxial growth of bi thin films on Ge(111). *Appl. Surf. Sci.* **256**, 1252–1256 (2009).
- <sup>33</sup> Payer, T. *et al.* High-quality epitaxial Bi(111) films on Si(111) by isochronal annealing. *Thin Solid Films* **520**, 6905–6908 (2012).
- <sup>34</sup> Hirahara, T. *et al.* Quantum well states in ultrathin Bi films: Angle-resolved photoemission spectroscopy and first-principles calculations study. *Phys. Rev. B* **75**, 035422 (2007).
- <sup>35</sup> Bian, G., Miller, T. & Chiang, T.-C. Electronic structure and surface-mediated metastability of Bi films on Si(111)-7×7 studied by angle-resolved photoemission spectroscopy. *Phys. Rev. B* **80**, 245407 (2009).
- <sup>36</sup> Takayama, A., Sato, T., Souma, S., Oguchi, T. & Takahashi, T. Tunable spin polarization in bismuth ultrathin film on Si(111). *Nano Letter* **12**, 1776–1779 (2012).
- <sup>37</sup> Ito, S. *et al.* Alkali-metal induced band structure deformation investigated by angle-resolved photoemission spectroscopy and first-principles calculations. *Phys. Rev. B* **97**, 155423 (2018).
- <sup>38</sup> Liu, Y. & Allen, R. E. Electronic structure of the semimetals Bi and Sb. *Phys. Rev. B* **52**, 1566 (1995).
- <sup>39</sup> Ohtsubo, Y. & Kimura, S.-i. Topological phase transition of single-crystal Bi based on empirical tight-binding calculations. *New J. Phys.* **18**, 123015 (2016).
- <sup>40</sup> Gonze, X. *et al.* First-principles computation of material properties: the ABINIT software project. *Comput. Mater. Sci.* **25**, 478–492 (2002).
- <sup>41</sup> Perdew, J. P., Burke, K. & Ernzerhof, M. Generalized gradient approximation made simple. *Phys. Rev. Lett.* **77**, 3865 (1996).
- <sup>42</sup> Hartwigsen, C., Goedecker, S. & Hutter, J. Relativistic separable dual-space gaussian pseudopotentials from H to Rn. *Phys. Rev. B* **58**, 3641 (1998).
- <sup>43</sup> Monkhorst, H. J. & Pack, J. D. Special points for Brillouin-zone integrations. *Phys. Rev. B* **13**, 5188 (1976).
- <sup>44</sup> Giannozzi, P. *et al.* QUANTUM ESPRESSO: a modular and open-source software project for quantum simulations of materials. *J. Phys. Condens. Matter* **21**, 395502 (2009).
- <sup>45</sup> Yukawa, R., Ozawa, K., Yamamoto, S., Liu, R.-Y. & Matsuda, I. Anisotropic effective mass approximation model to calculate multiple subband structures at wide-gap semiconductor surfaces: Application to accumulation layers of SrTiO<sub>3</sub> and ZnO. *Surf. Sci.* **641**, 224–230 (2015).